Available online at www.sciencedirect.com
ScienceDirect
Polymer 48 (2007) 4466–4481
polymer
www.elsevier.com/locate/polymer

Aggregation behaviors and photoresponsive properties of azobenzene constructed phosphate dendrimers

Wenquan Zhang, Jianda Xie, Zhu Yang, Wenfang Shi*

Department of Polymer Science and Engineering, University of Science and Technology of China, Hefei, Anhui 230026, PR China

Received 16 March 2007; received in revised form 22 May 2007; accepted 23 May 2007
Available online 26 May 2007

Abstract

The first to third generation of amphiphilic azobenzene constructed phosphate dendrimers (*G*0 to *G*2) was synthesized via a convergent strategy and characterized by NMR and MALDI-TOF-MS measurements. The aggregation behaviors and photoresponsive properties of their aggregates in water were investigated. The TEM observation and UV–vis absorption spectral study showed that the morphologies of the aggregates are greatly affected by the preparation method. The multiple aggregation states, including H-aggregation and J-aggregation, were formed by azobenzene moieties in *G*1 and *G*2 aggregates prepared via sonication, which was thought to be due to their different distance from the hydrophilic phosphate group. The controlled release property of *G*1 vesicle was investigated using calcein as a fluorescence indicator, showing the potential use as a photoregulatable carrier.

Keywords: Azobenzene; Dendrimer; Aggregation

1. Introduction

Azobenzene moieties can readily undergo reversible *trans–cis* photoisomerization, leading to the large structural change as reflected in the dipole moment, spatial requirement, and absorption spectra, which makes azobenzene moieties good candidates as a light-induced ''molecular switch'', and have been attracting increasing interest for many applications [1]. Azobenzene-containing amphiphiles can self-assemble into a variety of aggregates in aqueous solutions as micelles or different types of bilayer structures. The aggregates show interesting light-responsive behaviors including controllable membrane permeability [2–5], photoresponsive micelles [6–10] and change in fluorescence/absorbance spectroscopy [11,12]. In the aggregates, the strong aggregation of azobenzene chromophores was often observed on the basis of the spectral shift of the maximum absorption band. The blue shift of the maximum absorption band for azobenzene moiety is usually assigned to the parallel head-to-head alignment of azobenzene chromophores, called H-aggregation. In contrast, the red shift is normally observed as the azobenzene chromophores are aggregated in a head-to-tail manner which is called J-aggregation. The aggregation state of azobenzene chromophore can greatly influence the morphologies of the formed aggregate.

In the past two decades, a new family of polymers, named dendrimers or dendritic polymers, with three-dimensional molecular architecture and possessing starburst topology, has been attracting increasing interest for many applications. Among their promising applications, the use in controlled release systems has attracted much attention. Dozens of dendrimers including polyesters [13], polyamidoamines [14], and polyamides [15] have been synthesized successfully. In most delivery systems, the control over release rate is an important aspect. These systems need to be sensitive to some specific external stimuli, such as pH [16–19], enzyme [20,21], irradiation [22–25], or temperature [26,27]. Many dendrimers with stimuli-responsive moieties have been designed, where azobenzene is an excellent candidate. However, there are only few

* Corresponding author. Fax: +86 551 3606630.
E-mail address: wfshi@ustc.edu.cn (W. Shi).

0032-3861/$ - see front matter © 2007 Elsevier Ltd. All rights reserved.
doi:10.1016/j.polymer.2007.05.056

examples related to azobenzene-containing dendrimers incorporated into self-assemble/aggregation and controlled release behaviors. Moreover, the azobenzene moieties are mostly located in the exterior or at the core of dendritic polymers [28–32]. To the best of our knowledge, although the synthesis of dendrimers with azobenzene group throughout the molecular architecture have been reported [33–36], no amphiphilic dendrimers skeleton-constructed with azobenzene moiety has been prepared. For an amphiphilic azobenzene constructed dendrimer, the azobenzene moieties can be considered to be located at different parts of the molecular architecture due to its compact structure, especially for the dendrimer of higher generation. As a result, azobenzene moieties may show different aggregation behaviors according to their distance from the hydrophilic group. Therefore, it is of interest to investigate the self-assemble and aggregation behaviors of azobenzene constructed dendrimers.

In this study, the convergent synthesis strategy of first to third generation of azobenzene constructed amphiphilic phosphate dendrimers was described. Their aggregation behavior in water, light-responsive properties, and the permeability of vesicles formed by the second generation of dendrimer were investigated by UV–vis and fluorescence spectral study and TEM observation.

2. Experimental

2.1. Materials

CBA, CPA (CPA-MEM) as monomers and dendrons G1–COOH, G2–COOH were synthesized in the previous work [37]. Ethylenediaminetetraacetic acid (EDTA, tetra sodium salt hydrate) was purchased from Sigma. 4-(2-Hydroxyethyl)-1-piperazineethanesulfonic acid (HEPES) and dialysis tubing (MD44 molecular weight cut off: 14,000) were purchased from Shanghai Sangon Biological Engineering Technology & Services Co., Ltd. Thionyl chloride was distilled before use. 4-Dimethylaminopyridine (DMAP) and all other reagents and solvents were purchased from Sinopharm Chemical Reagent Co., Ltd., and used as received. Milli-Q water was used at all the time.

2.2. Characterization

The NMR measurements were performed on a Bruker 300 MHz spectrometer with appropriate solvents. The MALDI-TOF-MS spectra were recorded on a Bruker Daltonics BIFLEX™ III time-of-flight mass spectrometer equipped with a nitrogen laser (337 nm) using 1,8,9-anthracenetriol as a matrix and NaI as a cationization agent. The UV–vis spectral measurements were carried out using a Shimadzu UV-2401pc ultraviolet–visible spectrometer. The excitation light of Shimadzu Fluorescence Spectroscopy RF-5301PC was used for irradiation of the samples. The fluorescence spectra were recorded on a SPEX Fluorolog 3 spectrometer. The size and size distribution of micelles in aqueous solution were measured by dynamic light scattering (DLS) carried out on a Malvern Zetasizer Nano ZS90 with a He–Ne laser (633 nm) and 90° collecting optics. All samples were filtered through Millipore 1.0 μm filter prior to measurements. All measurements were carried out at 25 °C, and data were analyzed by Malvern Dispersion Technology Software 4.20.

2.3. Synthesis

2.3.1. G0–OH

CBA of 2.00 g (6.71 mmol) was dispersed in 30 ml of CH_2Cl_2, followed by the addition of 2.20 g (18.49 mmol) $SOCl_2$ dropwise under stirring. The reaction was carried out for 4 h at room temperature, and at 40 °C for another 4 h under reflux condition till the reactant became a clear homogenous solution. Then CH_2Cl_2 and $SOCl_2$ were evaporated under vacuum carefully. The resulting red CBA acyl chloride was dissolved in 30 ml of CH_2Cl_2.

Glycol of 4.16 g (67.1 mmol) was dissolved in 40 ml of pyridine in the presence of DMAP (0.02 g) at 50 °C. The above prepared CBA acyl chloride solution was added dropwise into the glycol solution, and reacted for 8 h under stirring. After CH_2Cl_2 was removed by distillation, the reaction was further carried out for 8 h at 80 °C. The formed white pyridine salt was removed by filtration, and pyridine was evaporated under reduced pressure subsequently. The product mixture was then washed with 100 ml of water to get rid of most of unreacted glycol. Then the product was dissolved in 50 ml of $CHCl_3$, washed with water (3×100 ml), dried over Na_2SO_4 and concentrated under reduced pressure. The orange ceraceous product was obtained, named *G*0–OH (2.01 g, yield 87%).

*G*1–OH and *G*2–OH were obtained as orange powder and red powder, respectively, via a similar procedure as described for the synthesis of *G*0–OH, using *G*1–COOH and *G*2–COOH reacted with 10 equiv. glycol. Their yields were estimated to be 85% and 79%, respectively.

^{1}H NMR (300 MHz, $CDCl_3$) of *G*0–OH: $\delta = 1.00$ (t, $-CH_3$, 3H), 1.52 (m, $-CH_2CH_3$, 2H), 1.81 (m, $-CH_2CH_2CH_3$, 2H), 3.99 (t, $-OCH_2CH_2OH$, 2H), 4.06 (t, $-CH_2CH_2CH_2CH_3$, 2H), 4.51 (t, $-OCH_2CH_2OH$, 2H), 7.01 (d, Ar–H, 2H, *ortho* to O), 7.92 (m, Ar–H, 4H, *ortho* to N), 8.20 (d, Ar–H, 2H, *ortho* to –COO).

^{13}C NMR spectrum (75 MHz, $CDCl_3$, ppm) of *G*0–OH: $\delta = 13.93$ ($-CH_3$), 19.31 ($-CH_2CH_3$), 31.30 ($-CH_2CH_2CH_3$), 61.52 ($-OCH_2CH_2OH$), 67.00 ($-OCH_2CH_2OH$), 68.24 ($-OCH_2CH_2CH_2CH_3$), 114.92 (*o*-Ar*C* to $-OCH_2CH_2CH_2CH_3$), 122.47 (*m*-Ar*C* to $-OCH_2CH_2CH_2CH_3$), 125.32 (*m*-Ar*C* to –COO), 130.78 (*o*-Ar*C* to –COO), 131.05 (Ar*C* next to –COO), 146.97 (*p*-Ar*C* to $-OCH_2CH_2CH_2CH_3$), 155.62 (*p*-Ar*C* to –COO), 162.49 (Ar*C* next to $-OCH_2CH_2CH_2CH_3$), 166.24 (Ar*C*OO).

Anal. Calcd for $C_{19}H_{22}N_2O_4$: C, 66.65; H, 6.48; N, 8.18. Found: C, 66.77; H, 6.44; N, 8.17.

^{1}H NMR spectrum (300 MHz, $CDCl_3$, ppm) of *G*1–OH: $\delta = 1.00$ (t, $-CH_3$, 6H), 1.53 (m, $-CH_2CH_3$, 4H), 1.84 (m, $-CH_2CH_2CH_3$, 4H), 4.00 (t, Ar–C(O)–O–CH_2–CH_2, 2H),

4.06 (t, −CH_2CH$_2$CH$_2$CH$_3$, 4H), 4.51 (m, Ar−C(O)−O−CH_2−CH$_2$−O and Ar−O−CH_2−CH(O)−CH$_2$−O, 4H), 4.86 (m, Ar−O−CH$_2$−CH(O)−CH_2−O, 2H), 5.87 (m, Ar−O−CH$_2$−CH(O)−CH$_2$−O, 1H), 7.01 (d, Ar−H, 4H, *ortho* to O in CBA moiety), 7.11 (d, Ar−H, 2H, *ortho* to O in CPA moiety), 7.91 (m, Ar−H, 12H, *ortho* to N), 8.18 (m, Ar−H, 6H, *ortho* to −COO).

^{13}C NMR spectrum (75 MHz, CDCl$_3$, ppm) of *G*1−OH: $\delta = 13.95$ (−CH$_3$), 19.34 (−CH$_2$CH$_3$), 31.33 (−CH$_2$CH$_2$CH$_3$), 61.54 (−OCH$_2$$CH_2$OH), 63.37 (−O−CH$_2$−CH(O)−$CH_2$−O), 66.75 (−O−$CH_2$−CH(O)−CH$_2$−O), 67.00 (−O$CH_2CH_2$OH), 68.28 (−O$CH_2CH_2CH_2CH_3$), 70.60 (−O−CH$_2$−$C$H(O)−CH$_2$O), 114.92 (*o*-Ar*C* to O in CBA), 115.22 (*o*-Ar*C* to O in CPA), 122.49 (*m*-Ar*C* to O in CBA), 122.76 (*m*-Ar*C* to O in CPA), 125.41 (*m*-Ar*C* to −COO), 130.48, 130.58, 130.87, 131.03, 131.28, 131.32 (Ar*C* next and *ortho* to −COO), 147.00 (*p*-Ar*C* to −O in CBA), 147.61 (*p*-Ar*C* to O in CPA), 155.80 (*p*-Ar*C* to −COO), 161.40 (Ar*C* next to O in CPA), 162.58 (Ar*C* next to O in CBA), 165.56, 165.87 (Ar-*C*OO in CBA), 166.23 (Ar*C*OO in CPA).

Anal. Calcd for $C_{52}H_{52}N_6O_{10}$: C, 67.81; H, 5.69; N, 9.12. Found: C, 67.97; H, 5.44; N, 9.17.

^{1}H NMR spectrum (300 MHz, CDCl$_3$, ppm) of *G*2−OH: $\delta = 0.99$ (t, −CH_3, 12H), 1.52 (m, −CH_2CH$_3$, 8H), 1.82 (m, −CH_2CH$_2$CH$_3$, 8H), 4.00 (t, Ar−C(O)−O−CH$_2$−CH_2, 2H), 4.04 (t, −CH_2CH$_2$CH$_2$CH$_3$, 8H), 4.48 (m, Ar−C(O)−O−CH_2−CH$_2$−O and Ar−O−CH_2−CH(O)−CH$_2$−O, 8H), 4.84 (m, Ar−O−CH$_2$−CH(O)−CH_2−O, 6H), 5.85 (m, Ar−O−CH$_2$−CH(O)−CH$_2$−O, 3H), 7.00 (d, Ar−H, 8H, *ortho* to O in CBA moiety), 7.10 (d, Ar−H, 6H, *ortho* to O in CPA moiety), 7.92 (m, Ar−H, 28H, *ortho* to N), 8.18 (m, Ar−H, 14H, *ortho* to −COO).

^{13}C NMR spectrum (75 MHz, CDCl$_3$, ppm) of *G*2−OH: $\delta = 13.96$ (−CH$_3$), 19.35 (−CH$_2$CH$_3$), 31.34 (−CH$_2$CH$_2$CH$_3$), 61.54 (−OCH$_2$$CH_2$OH), 63.35 (−O−CH$_2$−CH(O)−$CH_2$−O), 66.75 (−O−$CH_2$−CH(O)−CH$_2$−O), 67.01 (−O$CH_2CH_2$OH), 68.28 (−O$CH_2CH_2CH_2CH_3$), 70.60 (−O−CH$_2$−$C$H(O)−CH$_2$O), 114.93 (*o*-Ar*C* to O in CBA), 115.21 (*o*-Ar*C* to O in CPA), 122.50 (*m*-Ar*C* to O in CBA), 122.76 (*m*-Ar*C* to O in CPA), 125.41 (*m*-Ar*C* to −COO), 130.50, 130.62, 131.88, 131.03, 131.29, 131.33 (Ar*C* next and *ortho* to −COO), 147.01 (*p*-Ar*C* to −O in CBA), 147.64 (*p*-Ar*C* to O in CPA), 155.81 (*p*-Ar*C* to −COO), 161.40 (Ar*C* next to O in CPA), 162.59 (Ar*C* next to O in CBA), 165.56, 165.87 (Ar-*C*OOCH$_2$−CH(O)), 166.24 (Ar*C*OOCH$_2$CH$_2$).

Anal. Calcd for $C_{118}H_{112}N_{14}O_{22}$: C, 68.20; H, 5.43; N, 9.44. Found: C, 68.56; H, 5.38; N, 9.38.

2.3.2. Dendrimers G0, G1, and G2

The double-azobenzene-chain phosphonate was obtained using the method represented in literature [38]. After the reaction of the hydroxyl group in *G*0−OH with PCl$_3$, the resonances of −O−CH_2−CH_2−O− in ^{1}H NMR spectra moved to higher chemical shifts. Moreover, resonance at around 8.52 appeared in the ^{31}P spectra after the reaction, which was related to phosphonate product.

The phosphate azobenzene dendrimer *G*0 was obtained using I$_2$ oxidation of the phosphonate [39]. After oxidation, the resonance of the phosphonate in ^{31}P NMR spectra moved to about −1.06 ppm. ^{1}H NMR spectrum was also measured to confirm that azobenzene moieties were not destroyed during the oxidation procedure. The final product was further purified by crystallization from EtOH resulting in orange crystals (yield 65%).

The phosphate dendrimers *G*1 and *G*2 were synthesized via a similar procedure. The product was purified by column chromatography (silica gel, eluents: CHCl$_3$/methanol (4:1) for *G*1 and CHCl$_3$/methanol (10:1) for *G*2). Red powder was obtained for *G*1 (yield 66%) and *G*2 (yield 56%).

^{1}H NMR spectrum (300 MHz, CDCl$_3$, ppm) of *G*0: $\delta = 1.00$ (t, −CH_3, 6H), 1.53 (m, −CH_2CH$_3$, 4H), 1.81 (m, −CH_2CH$_2$CH$_3$, 4H), 4.04 (m, −CH_2CH$_2$CH$_2$CH$_3$, 4H), 4.13 (t, P−O−CH_2, 4H), 4.56 (t, Ar−C(O)−O−CH_2−CH$_2$−O, 4H), 7.00 (d, Ar−H, 4H), 7.91 (m, Ar−H, 8H, *ortho* to N), 8.18 (m, Ar−H, 4H).

^{13}C NMR spectrum (75 MHz, CDCl$_3$, ppm) of *G*0: $\delta = 13.94$ (−CH$_3$), 19.32 (−CH$_2$CH$_3$), 31.31 (−CH$_2$CH$_2$CH$_3$), 63.23 (d, −OCH$_2$$CH_2$OP), 64.54 (d, −O$CH_2CH_2$OP), 68.24 (−O$CH_2CH_2CH_2CH_3$), 114.87 (*o*-Ar*C* to −OCH$_2$CH$_2$CH$_2$CH$_3$), 122.49 (*m*-Ar*C* to −OCH$_2$CH$_2$CH$_2$CH$_3$), 125.33 (*m*-Ar*C* to −COO), 130.78 (*o*-Ar*C* to −COO), 131.05 (Ar*C* next to −COO), 146.98 (*p*-Ar*C* to −OCH$_2$CH$_2$CH$_2$CH$_3$), 155.63 (*p*-Ar*C* to −COO), 162.50 (Ar*C* next to −OCH$_2$CH$_2$CH$_2$CH$_3$), 166.31 (Ar*C*OO).

^{31}P NMR spectrum (121 MHz, CDCl$_3$, ppm): $\delta = -1.06$.

^{1}H NMR spectrum (300 MHz, CDCl$_3$, ppm) of *G*1: $\delta = 1.00$ (t, −CH_3, 12H), 1.53 (m, −CH_2CH$_3$, 8H), 1.82 (m, −CH_2CH$_2$CH$_3$, 8H), 4.04 (m, −CH_2CH$_2$CH$_2$CH$_3$, 8H), 4.12 (t, P−O−CH_2, 4H), 4.50 (d, Ar−O−CH_2−CH(O)−CH$_2$−O, 4H), 4.55 (t, Ar−C(O)−O−CH_2−CH$_2$−O, 4H), 4.86 (m, Ar−O−CH$_2$−CH(O)−CH_2−O, 4H), 5.87 (m, Ar−O−CH$_2$−CH(O)−CH$_2$−O, 2H), 7.01 (d, Ar−H, 8H, *ortho* to O in CBA moiety), 7.11 (d, Ar−H, 4H, *ortho* to O in CPA moiety), 7.94 (m, Ar−H, 24H, *ortho* to N), 8.18 (m, Ar−H, 12H, *ortho* to −COO).

^{13}C NMR spectrum (75 MHz, CDCl$_3$, ppm) of *G*1: $\delta = 13.94$ (−CH$_3$), 19.32 (−CH$_2$CH$_3$), 31.31 (−CH$_2$CH$_2$CH$_3$), 63.21 (d, −OCH$_2$$CH_2$OP), 63.35 (−O−CH$_2$−CH(O)−$CH_2$−O), 64.62 (d, −O$CH_2CH_2$OP), 66.73 (−O−$CH_2$−CH(O)−CH$_2$−O), 68.25 (−O$CH_2CH_2CH_2CH_3$), 70.55 (−O−CH$_2$−$C$H(O)−CH$_2$O), 114.94 (*o*-Ar*C* to O in CBA), 115.19 (*o*-Ar*C* to O in CPA), 122.50 (*m*-Ar*C* to O in CBA), 122.75 (*m*-Ar*C* to O in CPA), 125.40 (*m*-Ar*C* to −COO), 130.84, 130.87, 131.03, 131.27, 131.33, 131.40 (Ar*C* next and *ortho* to −COO), 147.00 (*p*-Ar*C* to −O in CBA), 147.62 (*p*-Ar*C* to O in CPA), 155.66 (*p*-Ar*C* to −COO in CPA), 155.82 (*p*-Ar*C* to −COO in CBA), 161.43 (Ar*C* next to O in CPA), 162.58 (Ar*C* next to O in CBA), 165.56, 165.87 (Ar*C*OO in CBA), 166.32 (Ar*C*OO in CPA).

^{31}P NMR spectrum (121 MHz, CDCl$_3$, ppm) of *G*1: $\delta = -1.70$.

^{1}H NMR spectrum (300 MHz, CDCl$_3$, ppm) of *G*2: $\delta = 0.99$ (t, −CH_3, 24H), 1.53 (m, −CH_2CH$_3$, 16H), 1.81 (m, −CH_2CH$_2$CH$_3$, 16H), 4.03 (m, −CH_2CH$_2$CH$_2$CH$_3$, 16H), 4.10 (t, P−O−CH_2, 4H), 4.50 (d, Ar−O−CH_2−CH(O)−CH$_2$−O,

12H), 4.56 (t, Ar–C(O)–O–C*H*$_2$–CH$_2$–O, 4H), 4.85 (m, Ar–O–CH$_2$–CH(O)–C*H*$_2$–O, 12H), 5.86 (m, Ar–O–CH$_2$–C*H*(O)–CH$_2$–O, 6H), 7.02 (d, Ar–H, 16H, *ortho* to O in CBA moiety), 7.11 (d, Ar–H, 12H, *ortho* to O in CPA moiety), 7.94 (m, Ar–H, 56H, *ortho* to N), 8.19 (m, Ar–H, 28H, *ortho* to –COO).

^{13}C NMR spectrum (75 MHz, $CDCl_3$, ppm) of *G*2: $\delta = 13.95$ (–*C*H$_3$), 19.34 (–*C*H$_2$CH$_3$), 31.33 (–*C*H$_2$CH$_2$CH$_3$), 63.22 (d, –OCH$_2$*C*H$_2$OP), 63.37 (–O–CH$_2$–CH(O)–*C*H$_2$–O), 64.63 (d, –O*C*H$_2$CH$_2$OP), 66.75 (–O–*C*H$_2$–CH(O)–CH$_2$–O), 68.27 (–O*C*H$_2$CH$_2$CH$_2$CH$_3$), 70.58 (–O–CH$_2$–*C*H(O)–CH$_2$O), 114.95 (*o*-Ar*C* to O in CBA), 115.22 (*o*-Ar*C* to O in CPA), 122.51 (*m*-Ar*C* to O in CBA), 122.75 (*m*-Ar*C* to O in CPA), 125.40 (*m*-Ar*C* to –COO), 130.85, 130.90, 131.13, 131.27, 131.33, 131.40 (Ar*C* next and *ortho* to –COO), 147.00 (*p*-Ar*C* to –O in CBA), 147.62 (*p*-Ar*C* to O in CPA), 155.65, 155.80 (*p*-Ar*C* to –COO), 161.43 (Ar*C* next to O in CPA), 162.58 (Ar*C* next to O in CBA), 165.54, 165.87 (Ar-*C*OOCH$_2$–CH(O)), 166.34 (Ar*C*OOCH$_2$CH$_2$).

^{31}P NMR spectrum (121 MHz, $CDCl_3$, ppm) of *G*2: $\delta = -2.33$.

2.4. Preparation of aggregates

The aggregates were prepared using dilution and sonication methods. In the dilution approach, the dendrimer was dissolved in THF with an initial concentration of 1.5 mg/ml. Then 0.5 ml of the dendrimer solution was slowly added into 20 ml of water under stirring, and allowed further stirring for 10 min. In the sonication approach, an appropriate amount of dendrimer was dissolved in $CHCl_3$ and rotary-evaporated in a tube to obtain a thin film, which was dried in vacuum for 2 h. Then a small amount of water was added, and the mixture was vortexed at 70 °C for 10 min, followed by sonication at 70 °C for 15 min until a homogenous solution was obtained. The calcein release experiment was carried out according to the method described by Kuiper et al. [5], except that the non-encapsulated calcein was lastly removed by dialysis.

2.5. Transmission electron microscopy

The morphologies of vesicles were observed with a Hitachi-800 microscope. The high-resolution transmission electron

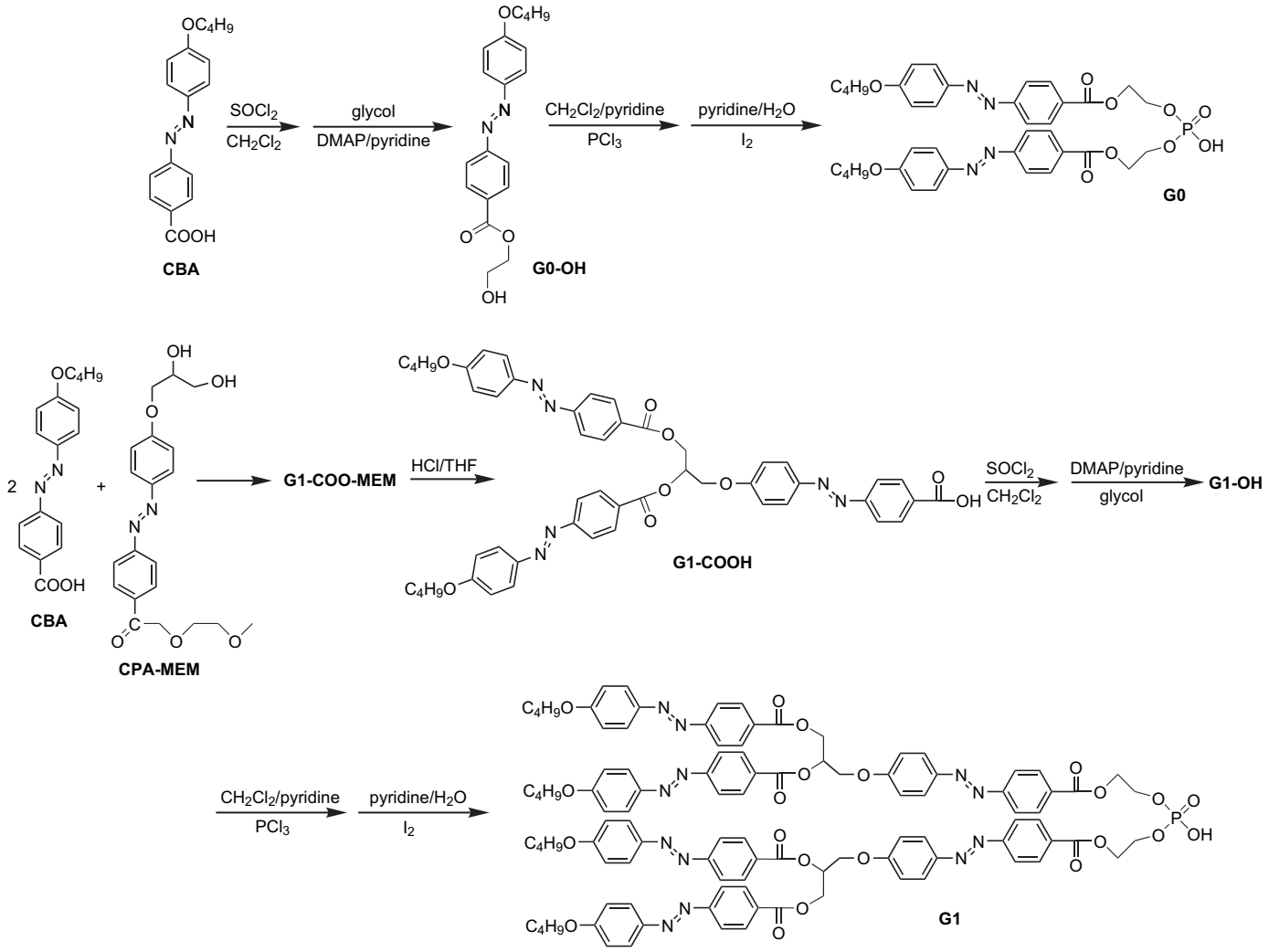

Scheme 1. Synthetic routes and chemical structures of dendrimers *G*0 and *G*1.

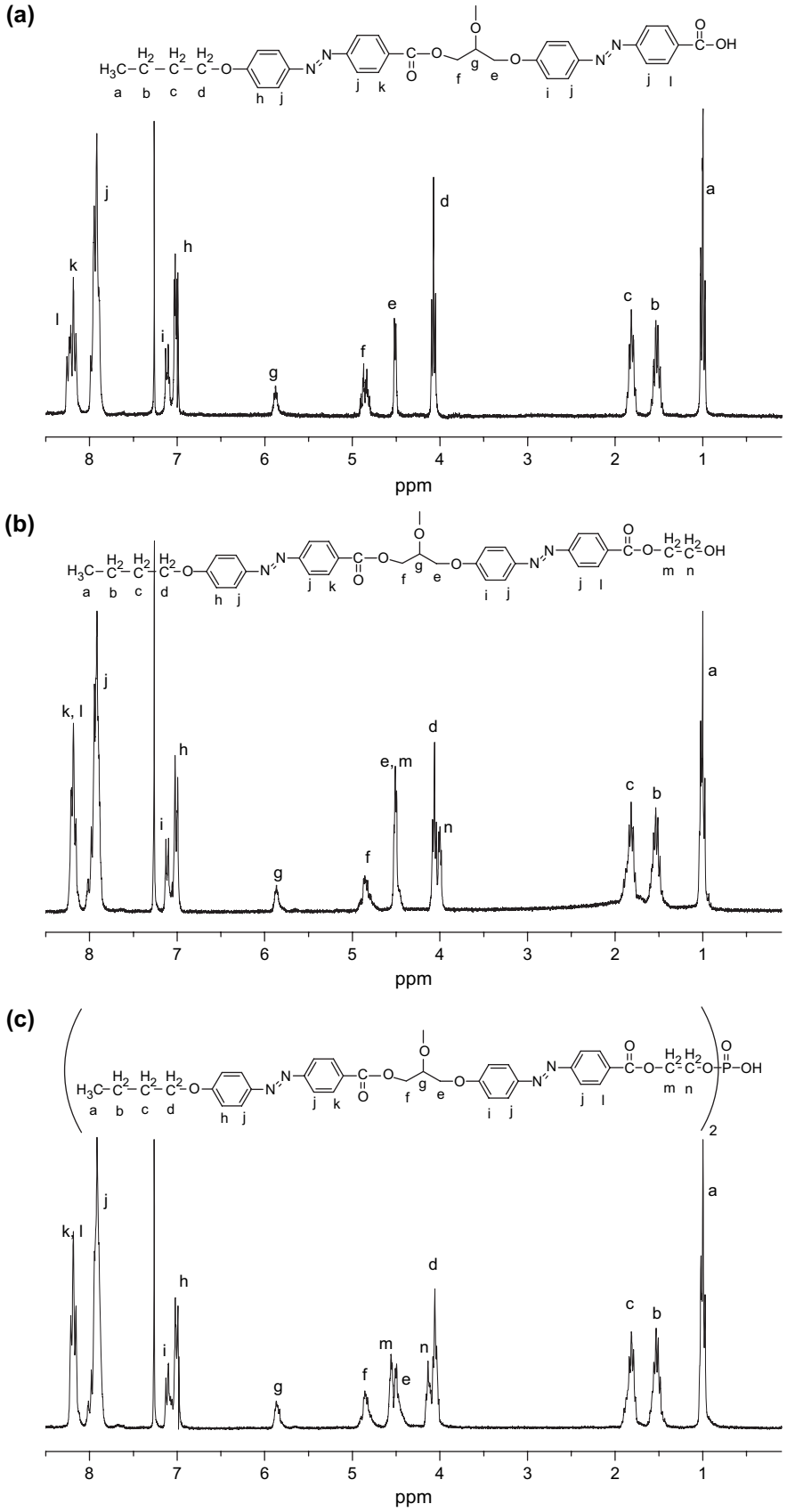

Fig. 1. ^{1}H NMR spectra of (a) *G*1−COOH, (b) *G*1−OH, and (c) *G*1 in $CDCl_3$.

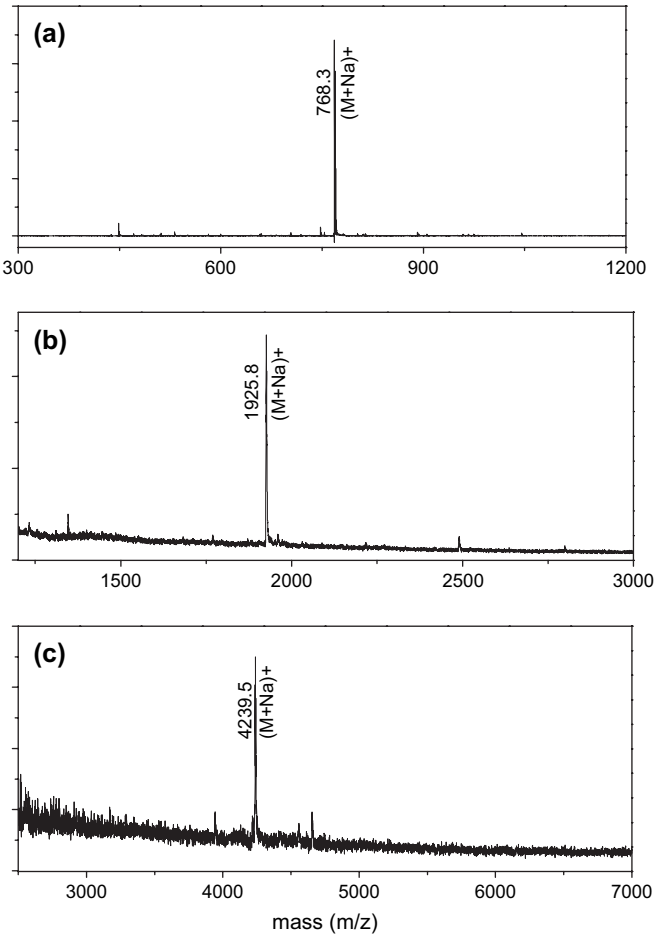

Fig. 2. MALDI-TOF mass spectra of (a) *G*0, (b) *G*1, and (c) *G*2.

microscopy (TEM, JEOL-2010) with a voltage of 200 kV was also utilized. To prepare samples for TEM observations, one drop of the aggregates' solution was cast on a carbon-coated copper grid and then immediately quenched with liquid nitrogen and freeze-dried (−50 °C).

3. Results and discussion

3.1. Characterization

The synthetic route and the chemical structure of dendrimers *G*0 and *G*1 are shown in Scheme 1.

The ^{1}H, ^{13}C and ^{31}P NMR spectra were utilized to track the synthetic procedure and confirm the formation of the dendrimers. The ^{1}H NMR spectra of *G*1−COOH, *G*1−OH, and *G*1 are shown in Fig. 1. The resonances of protons in

Table 1
Molecular weight of synthesized dendrimers measured by MALDI-TOF-MS compared with the calculated data

	*G*0	*G*1	*G*2
m/*z* (calcd)[a]	768.3	1924.7	4237.6
m/*z* (found)	768.3	1925.8	4239.5

[a] Calculated for $[M + Na]^{+}$.

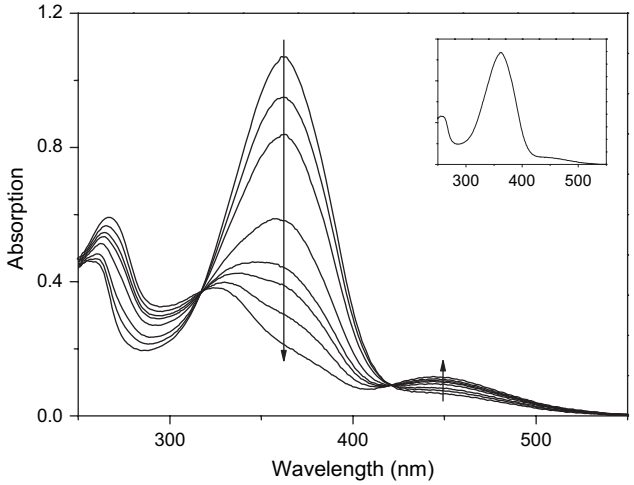

Fig. 3. UV−vis spectra of *G*1 (0.01 mg/ml in THF) after different irradiation times (360 nm; irradiation time: 0 s, 10 s, 20 s, 40 s, 80 s, 120 s, 160 s, and 240 s). Inset: UV−vis spectrum of *G*1 after 180 s irradiation with 450 nm.

1,2-propanediolether moiety (Ar−O−CH_2^e−CH^g(O)−CH_2^f(O)) in CPA originally appeared at $\delta = 3.48$ (e), 3.84 (g), 4.02 and 4.14 (f) ppm are moved to around $\delta = 4.52$ (e), 4.87 (f), and 5.88 (g) ppm for *G*1−COOH, which indicates the consumption of hydroxyl groups in CPA and the formation of dendron. Likewise, comparing the ^{1}H NMR spectrum for *G*1−OH with that for *G*1, it can be found that the changes in the chemical shifts related to the methylene protons (marked with ''m'' and ''n'') in glycol moiety also give an evidence that all the hydroxyl groups of *G*1−OH were reacted. The ^{31}P NMR spectra were utilized to confirm the formation of phosphate dendrimers.

The exact molecular weights of the phosphate dendrimers were measured using MALDI-TOF mass spectroscopy, as shown in Fig. 2. The experimental and theoretical *m*/*z* values are depicted in Table 1. All the experimental results are in good agreement with the expected molecular weights. Associated with the NMR results, the conclusion can be drawn that the purity of the final products is rather high.

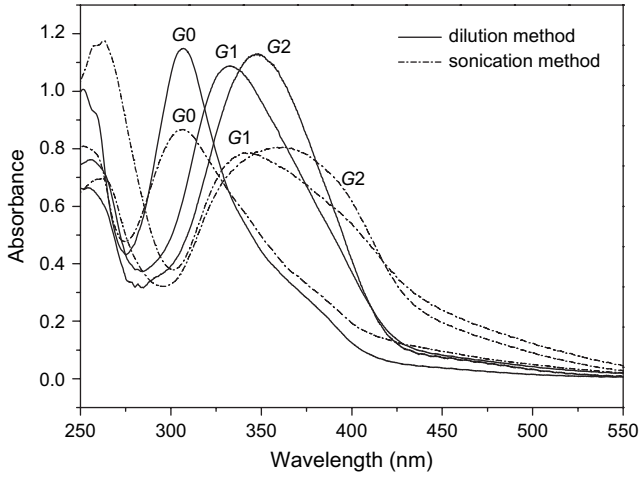

Fig. 4. UV−vis spectra of the aggregates prepared using dilution and sonication methods.

Table 2
Wavelength of maximal absorbance for dendrimers in THF and aggregates prepared using dilution and sonication methods

	In THF (nm)	Dilution method (nm)	Sonication method (nm)
*G*0	360	305	306
*G*1	360	330	340
*G*2	360	346	–

3.2. Light-responsive properties of dendrimers in THF

The UV–vis spectra of azobenzene phosphate dendrimers in THF all have maximum absorption at 360 nm related to the π–π* transition of azobenzene moiety. Fig. 3 shows the UV–vis spectral changes of *G*1 in THF upon irradiation at 360 nm for different times. It can be seen that as *G*1 was irradiated with 360 nm light to induce the *trans–cis* isomerization, the photostationary state was attained within 300 s. After that almost all azobenzene moieties take a *cis* isomer. Moreover, the *trans–cis* isomerization of azobenzene moiety is fully reversible when exposed to visible light at around 450 nm, as shown in the inset spectrum of Fig. 3.

3.3. Aggregation behavior of the dendrimers

Two methods including dilution and sonication were utilized to prepare the aggregates in order to investigate the aggregation behaviors of the dendrimers in water. It was found that the morphologies and UV–vis spectra of the aggregates are distinctly different for the different generations of dendrimers using two preparation methods.

The UV–vis spectra of the aggregates prepared using both methods are shown in Fig. 4. The maximum absorption band of the aggregate dispersion was used to characterize the aggregation state of azobenzene moiety. The absorption spectra of the aggregates prepared by dilution method are different from that by sonication, especially for *G*1 and *G*2 aggregates, indicating that the different aggregation states are formed from two preparation approaches. When using the dilution method, the maximum absorption bands of the dendrimers all show

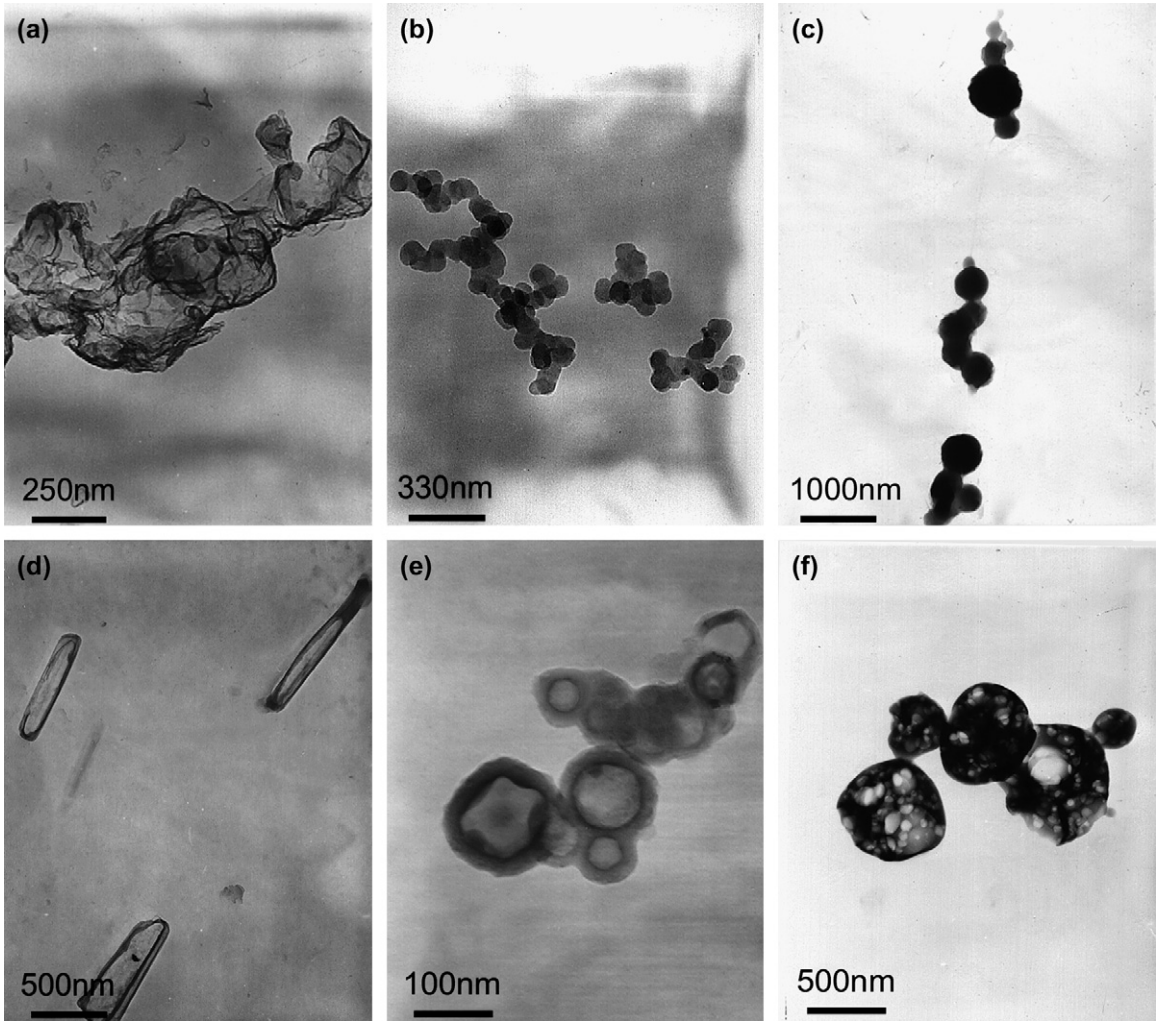

Fig. 5. TEM images of the aggregates for (a) *G*0, (b) *G*1 and (c) *G*2 prepared by the dilution method and (d) *G*0, (e) *G*1 and (f) *G*2 prepared by the sonication method.

Table 3
Hydrodynamic diameters for aggregates prepared using dilution and sonication methods

	Dilution method (d, nm)	Sonication method (d, nm)
$G0$	183	295
$G1$	76	91
$G2$	162	371

blue shifts (Table 2), indicating the formation of H-aggregation. Moreover, with the increase of generation of dendrimer, it was found that they formed looser H-aggregation state. The increase of generation of the dendrimer will lead to more compact molecular architecture, which will influence the aggregation state in two aspects. One is that the distance of adjacent azobenzene moieties decreased with the increase of generation. The other is that the azobenzene moieties are harder to orient freely to form H-aggregation. In our system, there are only two carbon atoms between azobenzene moieties grown from the same focal point. It is more difficult for the azobenzene moieties oriented to form H-aggregation state with adjacent ones. Hence, the aggregation state was thought to be mainly formed by azobenzene from different molecules. And the looser aggregation state was formed due to the more branched molecular structure and the relevant larger steric hindrance effect for higher generation dendrimers. The maximum absorption of $G0$ aggregates prepared by two methods both shows a large blue shift by about 55 nm compared with the

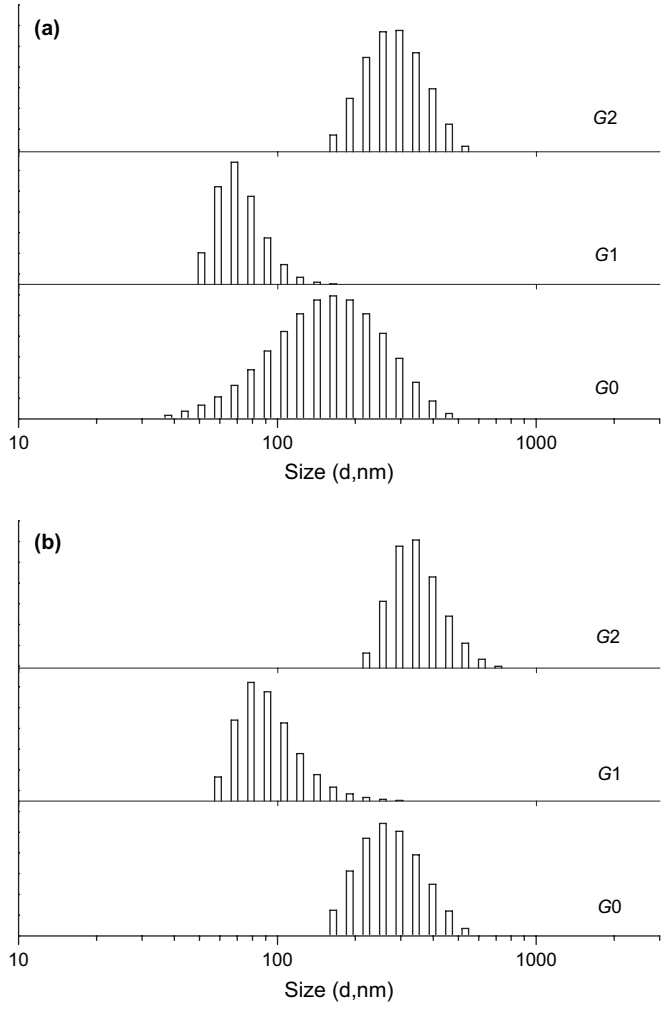

Fig. 6. Hydrodynamic diameter distribution of aggregates prepared by (a) dilution method and (b) sonication method.

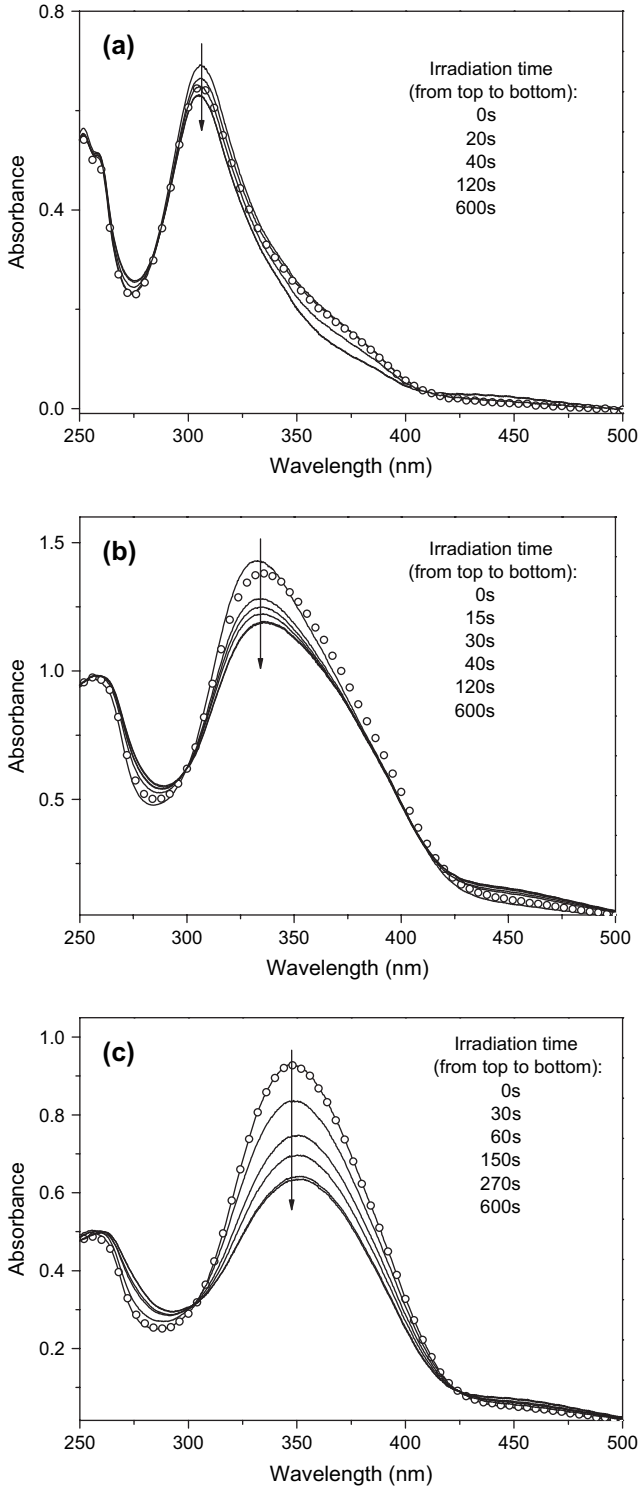

Fig. 7. UV–vis spectra of aggregates prepared by the dilution method for (a) $G0$, (b) $G1$ and (c) $G2$ after 360 nm light irradiation (—) for different times and subsequently 460 nm light irradiation (○).

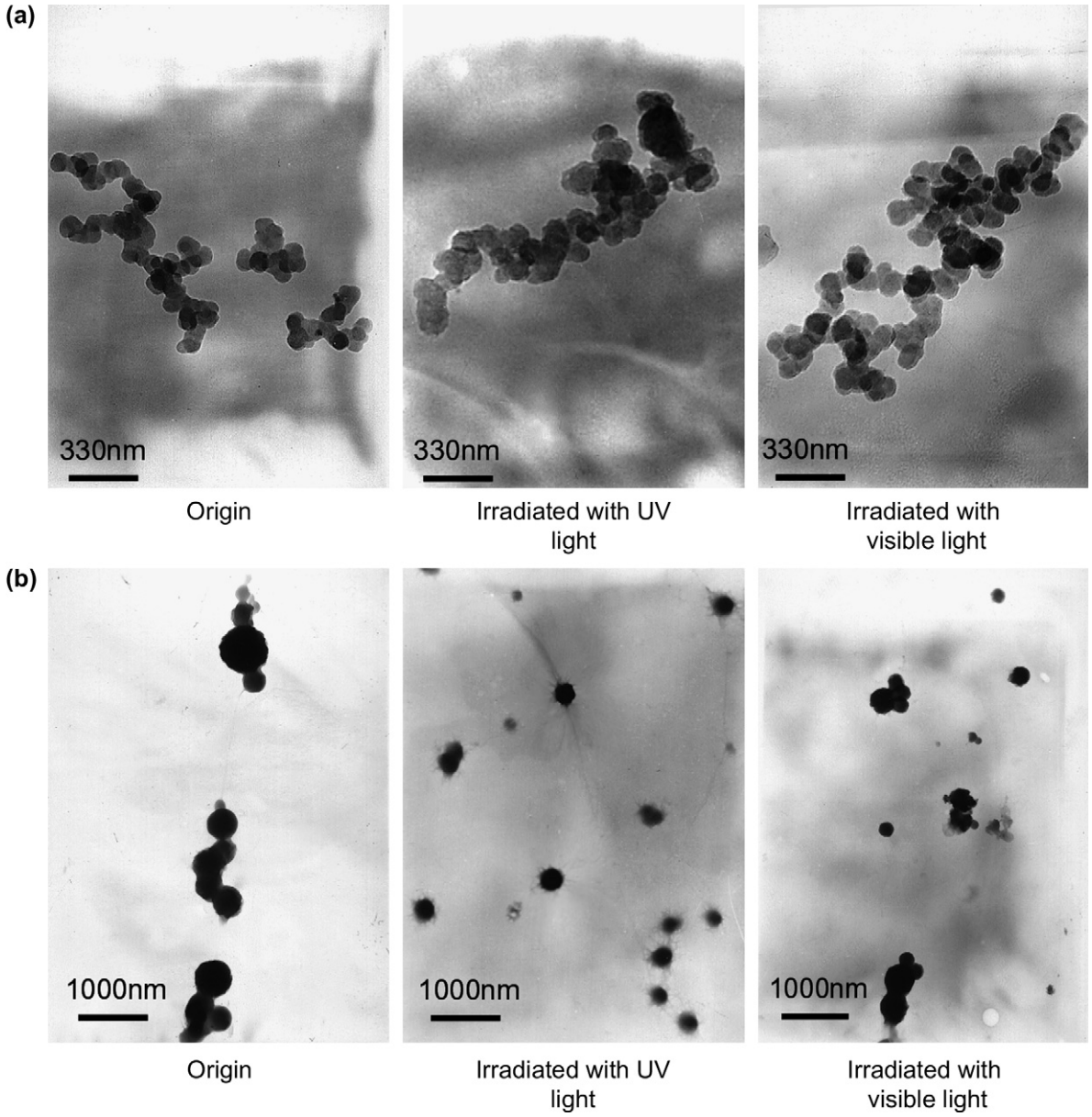

Fig. 8. TEM images for the morphological changes of (a) *G*1 and (b) *G*2 aggregates prepared by the dilution method after UV light irradiation and subsequent visible light irradiation.

corresponding band (360 nm) of its THF solution, which indicates that H-aggregation of azobenzene chromophores is formed in the aggregates. For dendrimer *G*1, no such strong H-aggregation was found. The maximum absorption of aggregates prepared by the dilution method blue shifts about 30 nm, but that of aggregates prepared by the sonication blue shifts only about 20 nm. Furthermore, the latter is wider than that of the former, having a shoulder peak occurred at around 395 nm. The reasonable interpretation is that when using the dilution method, the swift change in the environment surrounding the amphiphilic molecules drives the azobenzene chromophores congregated rapidly, and the difference in the hydrophilicity of the chromophores failed to establish the more thermodynamic stable aggregates. While using the sonication method, the more thermodynamic stable state was obtained with not only parallel ''head-to-head'' H-aggregation, but also tilted ''head-to-tail'' J-aggregation according to their hydrophilic ability. However, for *G*2 aggregates prepared by the dilution method, the maximum absorption band blue shifted about 14 nm, indicating the formation of a more loosely packed H-aggregation state by the azobenzene moiety. Moreover, *G*2 aggregates prepared by the sonication method show a broader absorption band from 320 nm to 400 nm, suggesting that the multiple aggregation states of azobenzene chromophores were formed.

Fig. 5 shows the TEM images for the morphologies of the aggregates prepared by both methods. Using the dilution method, *G*0 aggregates in the aqueous dispersion show a very flat bilayer structure (Fig. 5a). The strong H-aggregation state of the chromophores was thought to resist the

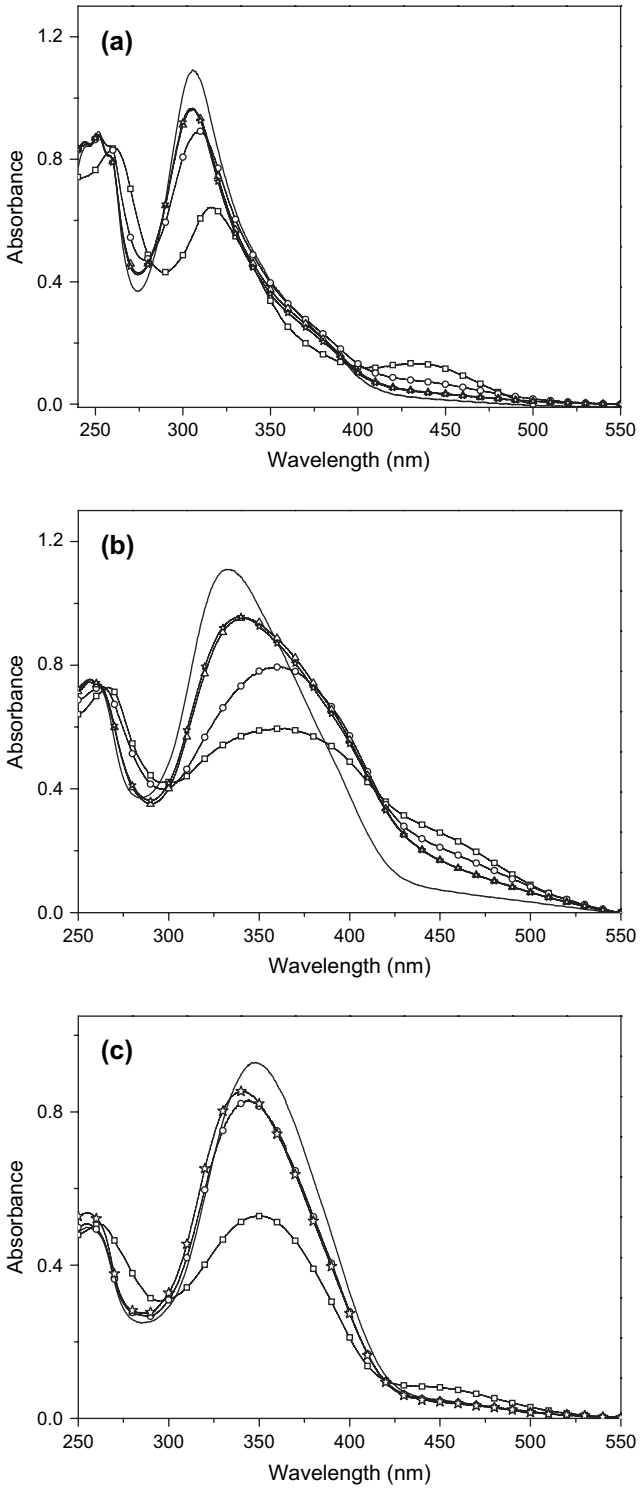

Fig. 9. UV–vis spectra of the formed *cis*-isomer aggregates and the spectral changes in the thermal recovery *cis–trans* process for (a) *G*0, (b) *G*1, and (c) *G*2: (□) *cis*-isomer aggregates, (○) after 12 h, (△) after 1 day, and (☆) after 5 days; for comparison, the spectra of formed *trans*-isomer aggregates are also given (—).

necessary curvature that would be required to form a small unilamellar or spherical structure [3]. However, *G*1 and *G*2 both give spherical structures, with different sizes and morphologies. *G*1 gives more perfect spheres than *G*2 with the diameter of around 70 nm (Fig. 5b). Whereas *G*2 self-assembled into much larger spherical aggregates but not as perfect as *G*1 with the diameter in the range of several hundred nanometers. They are loosely packed with the porous structure on the surface. The length of the long axis of *G*1 molecule is about 4 nm and that of *G*2 is below 8 nm. It may be concluded that such big difference in the aggregate sizes for *G*1 and *G*2 could not be attributed to their different molecular sizes. The hydrophilicity of molecules, density of chromophores, and the molecular structures all lead to the different aggregate sizes. The poorer hydrophilic property and more chromophores in one molecule make *G*2 easier to congregate and form larger aggregates. Furthermore, the *G*1 aggregates could not be classified as crew-cut micelles because the diameter of the aggregates is much larger than that of *G*1 molecule. The spherical aggregates are thought to possess a bilayer onion structure [40]. For *G*2, the highly branched structure associated with a relatively smaller hydrophilic group makes it much difficult to form a similar bilayer structure in such a rapid process, and thus the looser assemblies were formed.

The TEM images of the aggregates prepared by sonication are also given in Fig. 5. *G*0 aggregates was spindly vesicles, which can be regarded as rolled dispersion of the flat bilayer structure formed during the sonication. *G*1 gives vesicles. The thickness of the vesicles' membrane is estimated to be about 10 nm, indicating that the membrane possesses a typical bilayer structure. For *G*2, the porous spherical vesicles are observed.

The sizes of the formed aggregates were also confirmed by using dynamic light scattering measurement. The average hydrodynamic diameters obtained are listed in Table 3. Compared the results with that from TEM measurements, it can be found that two results fit well, which corroborates the interpretation given for the TEM images. The distributions of hydrodynamic diameters obtained are presented in Fig. 6 for all the dendrimers prepared using both methods. As shown in Fig. 6, the size distributions of samples prepared by sonication method (Fig. 6b) are basically narrower than those prepared by dilution method (Fig. 6a). This may be due to that when using sonication method, the aggregation process of the amphiphilic dendrimers is slower and it is easier for the dendrimers to form more stable aggregates with narrower distribution.

3.4. Light-responsive properties of aggregates

As the interaction among the *trans*-azobenzene chromophores plays an essential role during the aggregation process, the light-induced *trans–cis* isomerization may weaken the mechanical stability, resulting in the morphological change of the aggregates. To investigate the possible light-induced structural changes in the aggregates, the particular emphasis was placed on their spectral and morphological changes. In addition, for all aggregates in aqueous dispersions, despite the preparation method, it was found that due to the interaction between the azobenzene chromophores, the photoisomerization could not be completely achieved and a part of

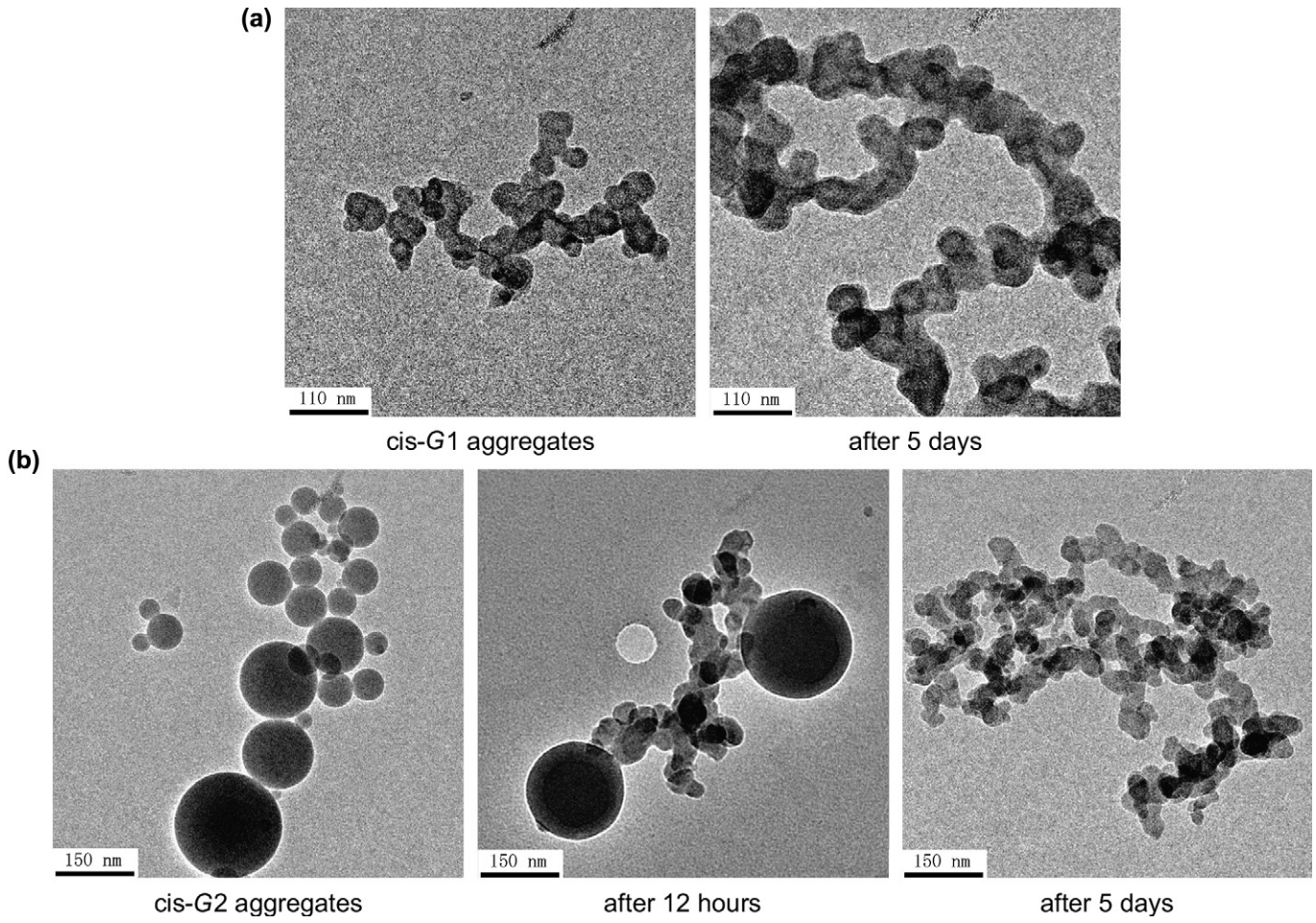

Fig. 10. TEM images for the morphologies of (a) *G*1 and (b) *G*2 freshly prepared *cis*-isomer aggregates by the dilution method, and after a period of thermal *cis*–*trans* isomerization process.

azobenzene groups still remain in *trans* state when the photostationary state was obtained.

3.4.1. Light-responsive properties of the aggregates prepared by the dilution method

The *G*0, *G*1, and *G*2 aggregates prepared by the dilution method were irradiated using the light of 360 nm until the photostationary state was obtained, and subsequently irradiated using visible light (460 nm). The changes in the UV–vis spectra with irradiation time are shown in Fig. 7. The decrease of absorbance at the maximum absorption band of the aggregates increases from *G*0 to *G*2 under UV light irradiation. This implies that the strong H-aggregation is difficult to be disrupted by irradiation for *G*0, which is observed as slight changes in the absorption spectra (Fig. 7a). For *G*1 and *G*2, the H-aggregation was weaker, more chromophores could take the *trans*–*cis* isomerization under UV light irradiation. The TEM images of the *G*1 and *G*2 aggregates after UV light and visible light irradiations are shown in Fig. 8. *G*0 showed no obvious change and thus the images were not given. For *G*1 aggregates, the spherical structure can be still observed, but the surface of spheres was slightly damaged and became loose and rough one after UV irradiation. However, for *G*2, the UV irradiation results in the significant change in their morphologies. The original spherical structure with porous surface became even more puffed and its average size decreased. The TEM images of the aggregates after sequential visible light irradiation are also shown in Fig. 8. All the morphological structures essentially recover to the initial ones despite the changes in UV–vis spectrum.

To fully understand the influence of the conformation of azobenzene chromophores on the morphologies of the aggregates, the aggregation behavior of fully *cis*-isomer dendrimers was also investigated. The dendrimer solution in THF was irradiated with 360 nm light to induce fully *trans*–*cis* isomerization of the chromophores and then the aggregates were prepared via the dilution method. The UV–vis spectra of the formed *cis*-isomer aggregates and the spectral changes from the thermal recovery *cis*–*trans* process are shown in Fig. 9. For comparison, the UV–vis spectra of directly formed *trans*-dendrimer aggregates are also given. It can be found that the thermal *cis*–*trans* isomerization of azobenzene results in a gradual blue shift of the maximum absorption band for all aggregates. Moreover, all spectra for the aggregates 5 days after preparation show difference compared with the directly formed *trans*-dendrimer aggregates. The difference between

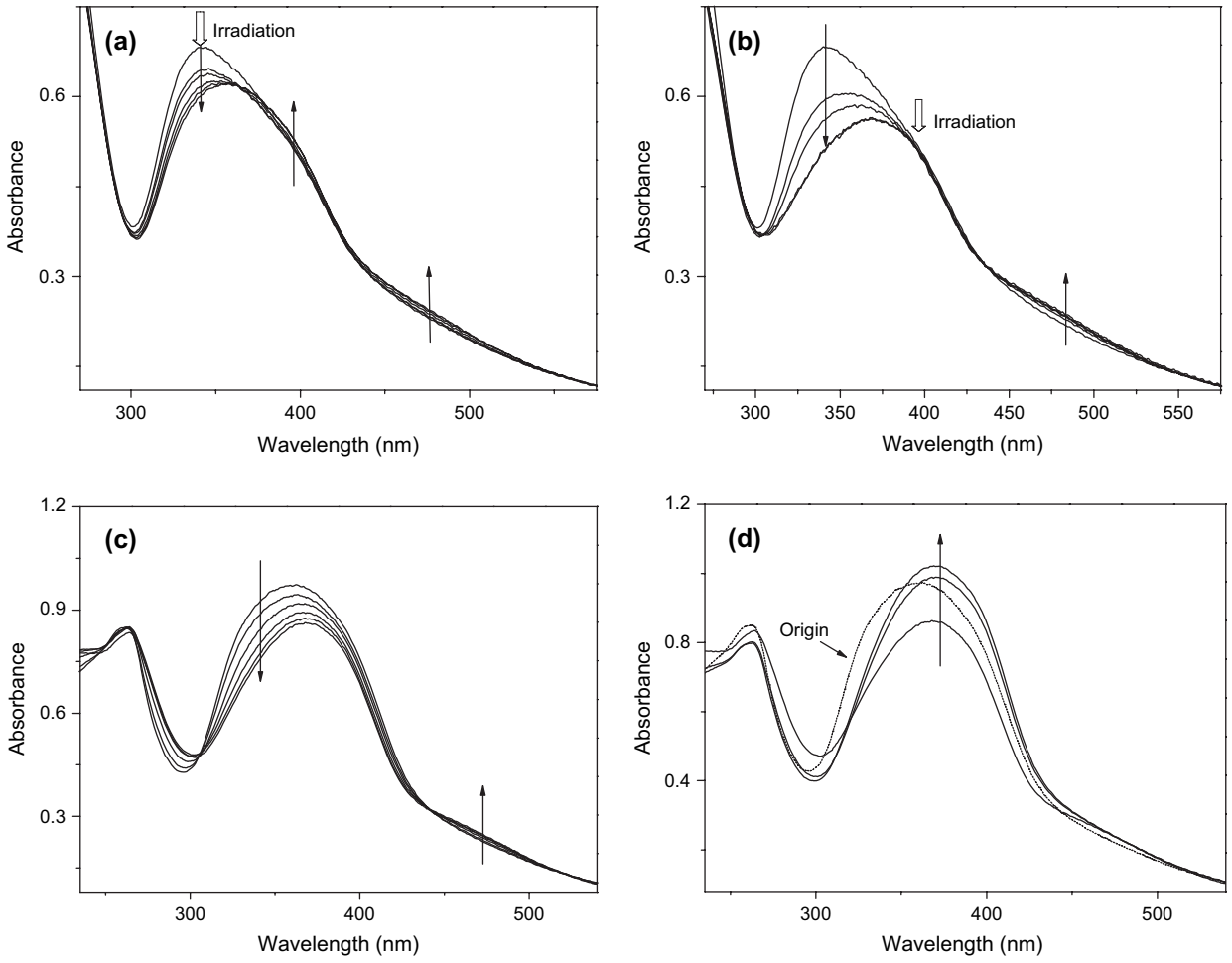

Fig. 11. UV–vis spectra of *G*1 aggregates under irradiation with (a) 340 nm and (b) 395 nm; UV–vis spectra of *G*2 aggregates under irradiation with (c) 360 nm and (d) subsequently 475 nm.

two aggregates of *G*0 is inconspicuous except for the slight raise of absorbance at 360 nm which may be attributed to the isolated *G*0 molecules (Fig. 9a). From Fig. 9b, the thermal *cis–trans* isomerization of azobenzene moiety in *G*1 results in a broader absorption band compared with that from the directly formed *trans*-dendrimer aggregates. This implies that the H-aggregation was also weaker than that of directly formed *trans*-dendrimer aggregates. The spectrum is very similar to that of *G*1 aggregates prepared by the sonication method (Fig. 4), which suggests that the similar aggregation manner of azobenzene moiety may be present in two aggregates. In contrast, from the narrower spectrum for *G*2 (Fig. 9c), even stronger H-aggregation than directly formed *trans*-dendrimer aggregates was obtained. The TEM images of the *cis*-isomers *G*1 and *G*2 aggregates freshly prepared and after the thermal recovery process are shown in Fig. 10. The solubility of *cis*-*G*0 was higher than that of *trans*-*G*0, so that no morphologies could be observed. As the *cis–trans* isomerization happened, the flat bilayer morphologies similar to *trans*-*G*0 were observed. From Fig. 10a, the *cis*-*G*1 gives a bilayer vesicle structure which is similar to the aggregates prepared by sonication method. The thermal recovery process did not greatly change its morphologies except for the slightly increased thickness of the membrane. For *cis*-*G*2, the large compound micelles (LCMs) were formed, as shown in Fig. 10b. These morphologies are thought to be similar to that formed by the amphiphilic PAA–PS blocked polymers [41,42]. When the azobenzene moieties took a *cis–trans* isomerization, the interaction between the chromophores was strengthened, which leads to the break of the equilibrium between amphiphilic dendrimer and solvent. The tighter aggregates were formed and phase-separated from the solution. Thus the continuous phase was broken, leading to the elimination of LCMs and the formation of small micelles during this process. When the TEM images (Fig. 10) are associated with the UV–vis spectral changes (Fig. 9), the possible explanation can be given for the difference in the aggregation behaviors of *G*1 and *G*2 aggregates. The interaction of *cis*-isomers is weaker than that of *trans*-isomers due to the decrease of π-conjugated region. The *cis*-dendrimer aggregates were formed mainly due to the hydrophilic/hydrophobic interaction and π–π interaction of the aromatic moieties which are obviously weaker than that of the azobenzene chromophores. The aggregation process for *cis*-isomer was slow than *trans*-isomer and

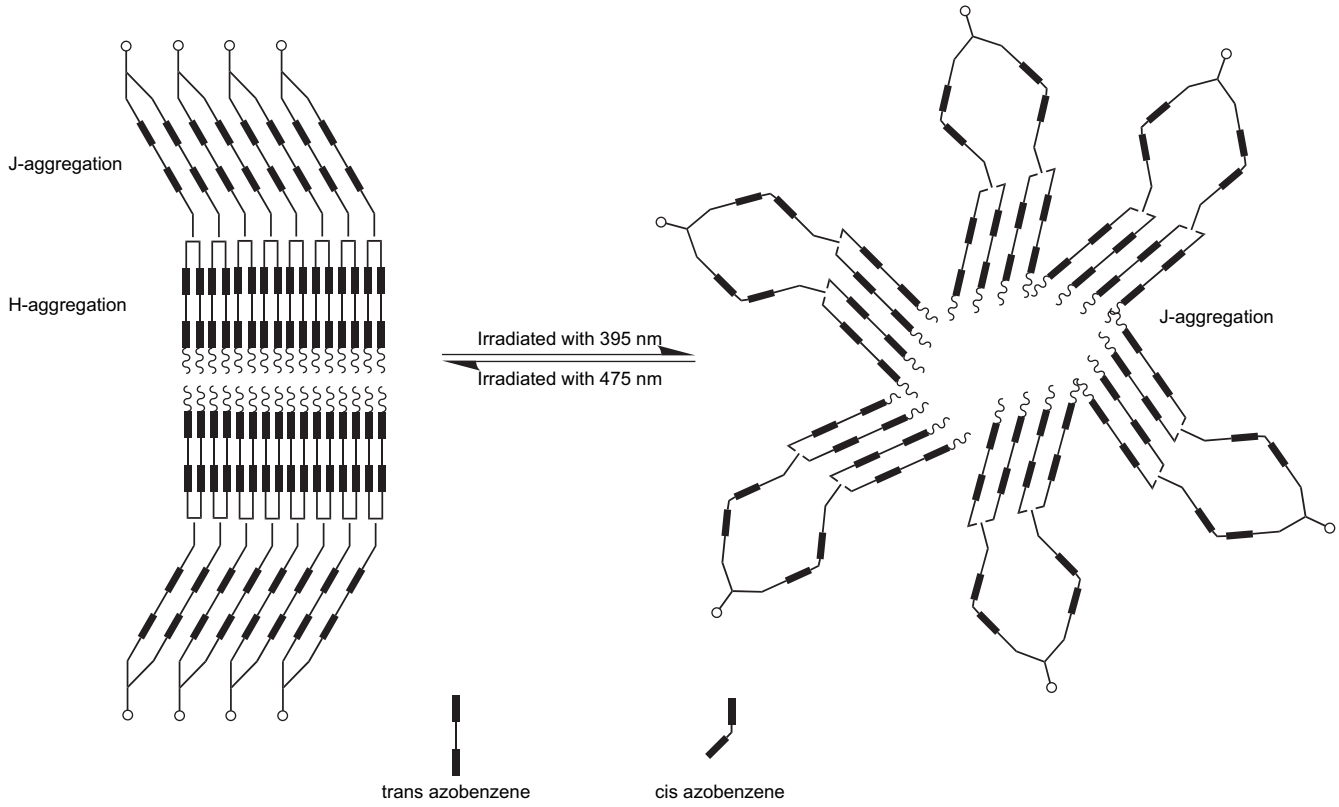

Scheme 2. Schematic illustration of the photoresponsive procedure for *G*1 aggregates built up with both H-aggregation and J-aggregation.

thus more thermodynamic stable aggregates could be formed. Therefore, for *cis*-*G*1, the slow aggregation process results in the bilayer vesicles (Fig. 10a). When the azobenzene moiety isomerizes back to *trans*, the bilayer vesicle structure still remains and the absorption spectrum is similar to that of aggregates prepared by sonication (Fig. 4). For *G*2, there are more than twice azobenzene moieties in one molecule and the hydrophilicity is weaker than *G*1. As a result, the π−π interaction plays a more important role during the aggregation process and LCMs were formed. When the azobenzene moiety isomerizes to *trans* state through the slow thermal process, the existed π−π interaction between the adjacent azobenzene moieties makes it easier to form a tighter H-aggregation state and leads to the elimination of the LCMs.

3.4.2. Light-responsive properties of the aggregates prepared by sonication method

The UV−vis spectra of aggregates prepared by sonication after different irradiation times are shown in Fig. 11. As the UV−vis spectrum of *G*1 shows a shoulder peak at 395 nm beside the maximum absorption band. The aggregate solution of *G*1 was exposed to 340 nm and 395 nm, respectively, to obtain a series of spectra. The exposure to 340 nm leads to an increase in the absorbance at 395 nm, 475 nm, and a decrease at 340 nm (Fig. 11a). However, when exposed to 395 nm, it was curiously found that the absorption at 340 nm greatly decreases as the exposure time was prolonged. Furthermore, little absorption change at 395 nm is observed, as shown in Fig. 11b. The possible explanation is that when exposed to 340 nm, the loosely packed H-aggregation in *G*1 was disrupted, which allowed the azobenzene chromophores to take *trans* to *cis* isomerization, resulted in the decrease at 340 nm and the increase at 475 nm. However, the isomerization was not fully completed, some of the released *trans*-azobenzene groups isolated during the break of H-aggregation formed J-aggregation, resulting in a increase at 395 nm. When exposed to 395 nm, the J-aggregation was disrupted and the azobenzene chromophores took the *trans* to *cis* isomerization, resulting in a increase at 475 nm. The decrease of absorbance at 340 nm revealed that the H-aggregation and J-aggregation are intercrossed together, which drove us to the presumption that the azobenzene chromophores in one phosphate dendrimer molecule may form different aggregation states due to the steric hindrance and difference in their positions. As the J-aggregation was disrupted and the azobenzene chromophores took *trans* to *cis* isomerization, the changes in geometry, van der Waals volume and dipole moment between *trans* and *cis* formation of the azobenzene moieties may influence the adjacent azobenzene moieties which are in H-aggregation state, and drive them to form the loose J-aggregation (Scheme 2). Both samples can be reversed to the original state when exposed to 475 nm, indicating that the changes in aggregation states are fully reversible.

The wavelength of 330 nm, 360 nm and 390 nm was utilized to induce *trans* to *cis* isomerization of *G*2 aggregates and all spectra show the similar trends. The UV−vis absorption spectra for *G*2 aggregates irradiated with 360 nm light are shown in Fig. 11c. The broad absorbance entirely shows

decrease with prolonged exposure time. Moreover, the absorption at around 345 nm decreases more quickly than that at around 370 nm. When the sample was subsequently exposed to 475 nm, it can be found that the absorption spectrum could not reverse to the original state (Fig. 11d). The absorption at 370 nm increases to a level even higher than that of original one, whereas that at 345 nm was not recovered. The conclusion may be drawn that the different aggregation states present at different positions in *G*2 architecture. Furthermore, it is difficult for the highly branched *G*2 molecules with comparatively low hydrophilicity to form the ordered morphologies such as lamella and vesicles during the aggregation. The less ordered aggregates are easy to be broken but hard to be restored.

The morphological changes of *G*1 and *G*2 aggregates prepared by sonication method under irradiation are given in Fig. 12. After UV irradiation, *G*1 vesicles show slight shrinkage and the thickness of membrane decreased. The subsequent visible light irradiation leads to fully restoration of the vesicles. For *G*2, the UV irradiation destroyed the porous spherical vesicles and resulted in the amorphous structures. However, the visible light irradiation was failed to restore the structures, which was in agreement with the UV–vis spectral results.

3.5. Photoregulated calcein release from G1 vesicles prepared by sonication

The controlled membrane permeability of *G*1 vesicles was investigated using calcein as a fluorescence indicator and no calcein leakage from the vesicles was observed for at least 15 days in dark. The aqueous dispersion of vesicles was irradiated for different times with appropriate wavelength. The release of calcein was monitored by tracking the emission intensity at 520 nm with the excitation at 490 nm. The total encapsulated calcein leakage was achieved by the addition of Triton-X-100 which was able to solubilize the vesicles.

As expected from the morphologies of *G*0 and *G*2 aggregates prepared by sonication, no calcein was found to be entrapped by comparing the emission spectra with or without the addition of Triton-X-100. As the *G*1 vesicles show both H-aggregation and J-aggregation, the light of both 340 nm and 395 nm were utilized to achieve the isomerization of

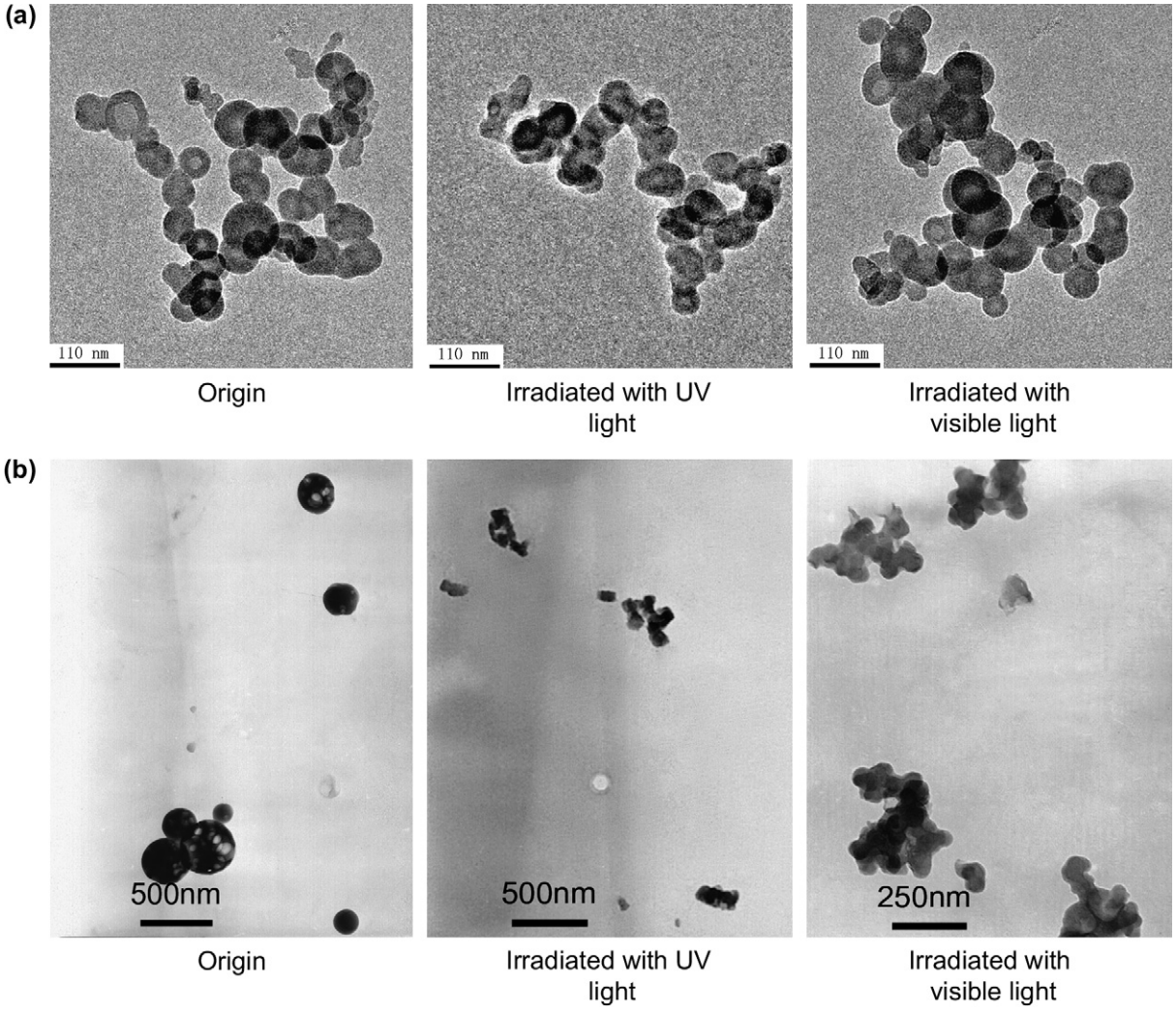

Fig. 12. TEM images for the morphological changes of (a) *G*1 and (b) *G*2 aggregates prepared by the sonication method under irradiation.

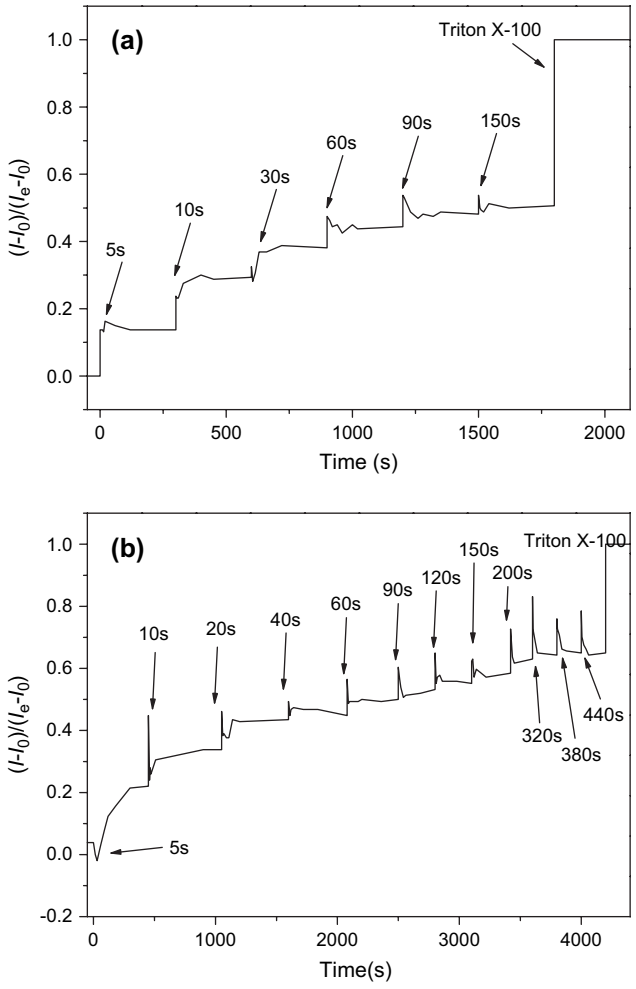

Fig. 13. Fluorescence profiles of the calcein release process upon irradiated as a function of time: (a) irradiated with 340 nm; (b) irradiated with 395 nm. (I_0, I_e, and I: initial intensity, final intensity after addition of Triton-X-100, and intensity at any time).

azobenzene chromophores. The leakage of calcein was detected right after irradiation and monitored for a period of time. Fig. 13 shows the fluorescence profiles of the calcein release process irradiated with both wavelengths. Because neither irradiation wavelengths could induce the fully *trans–cis* isomerization, only partial release of calcein could be achieved for both irradiation processes. When using 340 nm, it was found that the release rate was faster than that using 395 nm. However, the irradiation with 395 nm resulted in more leakage of calcein after a comparative long time irradiation. The previous studies have figured out that the isomerization of H-aggregation would lead to rapid release [3,5]. In our system, the irradiation with 340 nm can lead to direct isomerization of H-aggregation and cause rapid promotion of the membrane permeability. However, the irradiation with 395 nm can finally lead to the disruption of the H-aggregation as discussed above. The J-aggregation can be easily isomerized and lead to even more H-aggregation disrupted. This process was slower than that of direct H-aggregation isomerization but the final release portion of calcein was larger.

4. Conclusions

First to third generation of amphiphilic azobenzene constructed phosphate dendrimers (*G*0 to *G*2) was synthesized. The dendrimers can be easily dispersed in water to form the aggregates with different morphologies. The dendrimers tend to form looser structures with the increase of generation, and also related with the preparation method. For the *G*1 and *G*2 aggregates obtained via sonication, the multiple aggregation state can be established. Both H-aggregation and J-aggregation occurred for *G*1 vesicle using the sonication method. The *trans–cis* isomerization in the loosely packed J-aggregation can lead to the disruption of the H-aggregation efficiently. Therefore, it can be concluded that the different aggregation states were formed by the azobenzene moieties at different parts within one molecule, that is, the aggregation states are intercrossed together. The controlled release property of *G*1 vesicles was investigated using calcein as the fluorescence indicator, showing their potential use as a photoregulatable carrier.

Acknowledgment

The financial support from National Natural Science Foundation of China (No. 50633010) is gratefully acknowledged.

References

[1] Sudesh Kumar G, Neckers DC. Chem Rev 1989;89:1915.
[2] Okahata Y, Fujita S, Iizuka N. Angew Chem Int Ed Engl 1986;25:751.
[3] Song X, Perlstein J, Whitten DG. J Am Chem Soc 1997;119:9144.
[4] Sata T, Shimokawa Y, Matsusaki K. J Membr Sci 2000;171:31.
[5] Kuiper JM, Engberts JBFN. Langmuir 2004;20:1152.
[6] Wang G, Tong X, Zhao Y. Macromolecules 2004;37:8911.
[7] Deng YH, Li YB, Wang XG. Macromolecules 2006;39:6590.
[8] Jiang J, Tong X, Morris D, Zhao Y. Macromolecules 2006;39:4633.
[9] Ravi P, Sin SL, Gan LH, Gan YY, Tam KC, Xia XL, et al. Polymer 2005;46:137.
[10] Zhao H, Sand F, Masuda T. Polymer 2006;47:2596.
[11] Moss RA, Jiang W. Langmuir 1997;13:4498.
[12] Han M, Hara M. J Am Chem Soc 2005;127:10951.
[13] Gillies ER, Dy E, Fréchet JMJ, Szoka FC. Mol Pharmacol 2005;2:129.
[14] Quintana A, Raczka E, Piehler L, Lee I, Myc A, Majoros I, et al. Pharm Res 2002;19:1310.
[15] Fuchs S, Otto H, Jehle S, Henklein P, Schluter AD. Chem Commun 2005;14:1830.
[16] Hu H, Fan XD, Cao Zl. Polymer 2005;46:9514.
[17] Pistolis G, Malliaris A, Tsiourvas D, Paleos CM. Chem—Eur J 1999;5:1440.
[18] Sideratou Z, Tsiourvas D, Paleos CM. Langmuir 2000;16:1766.
[19] Feng X, Taton D, Borsali R, Chaikof EL, Gnanou Y. J Am Chem Soc 2006;128:11551.
[20] Wiwattanapatapee R, Lomlim L, Saramunee K. J Controlled Release 2003;88:1.
[21] Li X, Su Y, Chen Q, Lin Y, Tong Y, Li Y. Biomacromolecules 2005;6:3181.
[22] Yager KG, Barrett CJ. J Photochem Photobiol A Chem 2006;182:250.
[23] Shibaev V, Bobrovsky A, Boiko N. Prog Polym Sci 2003;28:729.
[24] Momotake A, Arai T. Polymer 2004;45:5369.
[25] Che P, He Y, Wang X. Macromolecules 2005;38:8657.
[26] Zhang JT, Huang SW, Zhuo RX. Macromol Biosci 2004;4:575.
[27] You YZ, Hong CY, Pan CY, Wang PH. Adv Mater 2004;16:1953.

[28] Mekelburger HB, Rissanen K, Vögtle F. Chem Ber 1993;126:1161.
[29] Archut A, Azzellini GC, Balzani V, De Cola L, Vögtle F. J Am Chem Soc 1998;120:12187.
[30] Li S, McGrath DV. J Am Chem Soc 2000;122:6795.
[31] Bobrovsky AYu, Pakhomov AA, Zhu XM, Boiko NI, Shibaev VP, Stumpe J. J Phys Chem B 2002;106:540.
[32] Atsuya M, Tatsuo A. Tetrahedron Lett 2004;45:4131.
[33] Yokoyama S, Nakahama T, Otomo A, Mashiko S. J Am Chem Soc 2000;122:3174.
[34] Sebastián RM, Blais JM, Caminade AM, Majoral JP. Chem—Eur J 2002;8:2172.
[35] Liao LX, Junge DM, McGrath DV. Macromolecules 2002;35:319.
[36] Wang S, Wang X, Li L, Advincula RC. J Org Chem 2004;69:9073.
[37] Zhang WQ, Xie JD, Shi WF. Eur Polym J 2007;43:2387.
[38] Kuiper JM, Hulst R, Engberts JBFN. Synthesis 2003;5:695.
[39] Garegg PJ, Regberg T, Stawinski J, Strornberg R. J Chem Soc Perkin Trans 1987;1269.
[40] Tsuda K, Dol GC, Gensch T, Hofkens J, Latterini L, Weener JW, et al. J Am Chem Soc 2000;122:3445.
[41] Yu Y, Eisenberg A. J Am Chem Soc 1997;119:8383.
[42] Cameron NS, Corbierre MK, Eisenberg A. Can J Chem 1999; 77:1311.